# Predictive ESO-based control with guaranteed stability for uncertain MIMO constrained systems

Alberto Castillo[a,*], Tito L.M. Santos[b], Pedro Garcia[a], Julio Elias Normey-Rico[c]

[a] *Instituto de Automática e Informática Industrial, Universitat Politècnica de València Valencia, Spain.*
[b] *Departamento de Engenharia Elétrica e de Computação (DEEC), Universidade Federal da Bahia (UFBA), Salvador-BA, Brazil.*
[c] *Universidade Federal de Santa Catarina, Florianopolis - SC, Brazil*

**Abstract**

In this paper, a novel predictive Extended State Observer (ESO)-based discrete controller with guaranteed stability is developed. Predictive controllers based on ESOs are gaining acceptance for controlling MIMO systems with disturbances, uncertainties or actuator constrains. However, one main concern about this control structure regards its closed-loop stability; which is not strictly guaranteed with the previous formulations. The proposed solution adds two new elements in the performance cost-index that permits to prove that –under the same assumptions that are normally taken in the ESO literature– the resulting closed-loop will be Input-to-State Stable against state-dependent uncertainties, observation errors and actuator constraints. A simulation case study of the glucose control in patients with type-1 diabetes is additionally included in order to illustrate the main advantages of this control structure.

*Keywords:* Extended State Observer (ESO); predictive control; uncertain systems; constrained systems.

## 1. Introduction

Disturbance rejection is one of the most fundamental problems in control, as every system may show uncertain behaviors that could have negative effects in feedback regulator [1]. These uncertain behaviors mostly arise from: mismatches between the nominal and the real system unmodeled or unknown dynamics, couplings with other systems, or unknown inputs that the system experiences during its operation –such as external forces or torques [2].

The Extended State Observer-Based Controllers (ESOBCs) are becoming one of the most popular solutions to mitigate the effect of these uncertainties [3, 4, 5, 6, 7, 8]. In particular, there is a current tendency to use predictive ESOBCs to reduce the uncertain behaviors of relatively complex systems, such as: uncertain MIMO systems with mismatch disturbances or hard control constraints [9]. Many works suggesting to employ predictive ESOBCs for these types of systems can be found, including applications such as: formation control of multiple robots [10], ultra-supercritical boiler-turbines [11], missile and lunar modules autopilots [12, 13], motion control of aerial drones and autonomous vessels [14, 9], wheeled inverted pendulum systems [15] and synchronous motors [16].

However, one main concern about predictive ESOBCs regards its closed-loop stability; which is not strictly guaranteed by the most part of previous formulations. In this sense, formulating a new predictive ESOBC with guaranteed stability is an important issue that should be tackled.

Therefore, this paper constructs a novel predictive ESO-based controller with guaranteed stability. The main contribution is to show that the closed-loop Input-to-State (ISS) stability is guaranteed –under the same assumptions that are normally taken in the ESO literature– if a fixed terminal-cost and a disturbance compensation terms are included in the cost-index.

The rest of the paper is structured as follows. Sec. 2 contains the problem formulation and some preliminaries. In Sec. 3, the predictive ESOBC is developed; whereas its closed-loop ISS is analyzed in Sec. 4. Sec. 5 aims to establish some relationships between this predictive controller and the so-called Generalized ESOBC [17]. Sec. 6 contains an illustrative simulation in order to highlight the advantages of this control approach if compared against conventional predictive controllers and non-predictive ESOBC. Finally, the main conclusions are summarized in Sec. 7.

### *1.1. Notation and definitions*

The following comparison functions are employed: **i)** a $\mathcal{K}$-function, $\gamma(\cdot) : \mathbb{R}^+ \to \mathbb{R}^+$; which is continuous and strictly increasing, with $\gamma(0) = 0$; **ii)** a $\mathcal{K}_\infty$-function, $\gamma_\infty(\cdot) : \mathbb{R}^+ \to \mathbb{R}^+$, which is a $\mathcal{K}$-function satisfying $\lim_{s\to\infty} \gamma(s) = \infty$; and **iii)** a $\mathcal{KL}$-function, $\beta(s,t) : \mathbb{R}^+ \times \mathbb{R}^+ \to \mathbb{R}^+$; which, for fixed $t$, is a $\mathcal{K}$-function in $s$; and, for a fixed $s$, it is decreasing in $t$, satisfying $\lim_{t\to\infty} \gamma(s,t) = 0$.

For any vector $x$ and any matrix $\Delta$ of appropriate dimensions: $\|x\| \triangleq \sqrt{x^T x}$, $\|x\|_\Delta \triangleq \sqrt{x^T \Delta x}$; while $\|\Delta\|$ denotes the corresponding induced-norm for matrices.

*Corresponding author
*Email addresses:* alcasfra@gmail.com (Alberto Castillo), titolms@gmail.com (Tito L.M. Santos), pggil@isa.upv.es (Pedro Garcia), julio.normey@ufsc.br (Julio Elias Normey-Rico)

Define $k \in \mathbb{N} \cup \{0\}$. For any function $\phi_k : k \to \mathbb{R}^a$, with $a \in \mathbb{N}$, denote $\phi_{[0,j]} \triangleq [\phi_0^T, \phi_1^T, \ldots, \phi_j^T]^T$, $j \in \mathbb{N}$; and $\|\phi_{[0,j]}\|_\infty \triangleq \sup\{\|\phi_k\| : k \in [0, j]\}$.

## 2. Problem formulation

Let us consider the following class of non-linear systems:

$$\begin{cases} \dot{x}(t) = Ax(t) + B_u u(t) + B_f f(x(t), \omega(t)), \\ y(t_k) = Cx(t_k); \quad t_{k+1} - t_k \triangleq h > 0, \end{cases} \tag{1}$$

where $x(t) = [x_1(t), \ldots, x_n(t)]^T \in \mathbb{R}^n$ is the system state; $y(t_k) \in \mathbb{R}^r$ is a discrete measurable output; $u(t) \in \mathbb{R}^m$ is the control action, which it is assumed to be restricted inside the closed-set $u_{min} \leq u(t) \leq u_{max}$, being $u_{max} \in \mathbb{R}^m$, $u_{min} \in \mathbb{R}^m$ its upper and lower bounds, respectively; $A \in \mathbb{R}^{n\times n}$, $B_u \in \mathbb{R}^{n\times m}$, $B_f \in \mathbb{R}^{n\times q}$, $C \in \mathbb{R}^{r\times n}$ are the nominal system matrices, being $A$ Hurwitz; $\omega(t) : \mathbb{R}_{\geq 0} \to \mathbb{R}^p$ is a differentiable time-varying function representing the external disturbances; $f : \mathbb{R}^n \times \mathbb{R}^p \to \mathbb{R}^q$ is a possibly non-linear function, differentiable in $\mathbb{R}^n \times \mathbb{R}^p$.

The function $f(x, \omega(t))$ is regarded as an unknown term representing the lumped effect of the internal uncertainties and the external disturbances.

Let us consider the following assumptions:

**Assumption 1.** There exists –unknown– scalars, $\epsilon_f \geq 0$, $\epsilon_{\dot{\omega}} \geq 0$, $\epsilon_{dx} \geq 0$, $\epsilon_{d\omega} \geq 0$, such that

$$\|f(x, \omega(t))\| \leq \epsilon_f, \qquad \|\dot{\omega}(t)\| \leq \epsilon_{\dot{\omega}}$$
$$\left\|\frac{\partial f}{\partial x}(x, \omega(t))\right\| \leq \epsilon_{dx}, \quad \left\|\frac{\partial f}{\partial \omega}(x, \omega(t))\right\| \leq \epsilon_{d\omega},$$

for all $x \in \mathbb{R}^n$, $t \geq 0$.

**Assumption 2.** For any initial state, $x(0)$, and any bounded $u(t)$, the solution of (1) satisfies that $\|x(t)\| \leq \epsilon_x$, $\forall t \geq 0$, $\epsilon_x \geq 0$.

**Assumption 3.** $u(t) = u_k$, $\forall t \in [t_k, t_{k+1})$.

Assumptions 1-2 are commonly employed in the ESO-based literature [18, 19, 20]. They basically say that the uncertain function $f(\cdot)$ is differentiable and it does not destabilizes the system (1). Assumption 3 states that the controller generates a discrete control action, $u_k$, at $t = t_k$, which is introduced to the system via ZOH –being normally the case in predictive ESOBCs.

*Discretized extended-state representation of system* (1)

In order to formulate the predictive ESOBC, system (1) needs to be firstly rewritten in a discretized extended-state representation:

**Proposition 1.** *Under Assumption 3, the system state and the lumped uncertainty at the sampling instants: $x(t_k)$, $f(x(t_k), \omega(t_k))$; are given by*

$$x(t_{k+1}) = \Phi x(t_k) + \Gamma_1 u_k + \Gamma_2 f(x(t_k), \omega(t_k)) + \mathcal{O}_{x,k}, \tag{2a}$$
$$f(x(t_{k+1}), \omega(t_{k+1})) = f(x(t_k), \omega(t_k)) + \mathcal{O}_{f,k}, \tag{2b}$$

*with $\Gamma_1 \triangleq \phi(h)B_u$, $\Gamma_2 \triangleq \phi(h)B_f$, $\phi(x) \triangleq \sum_{i=1}^{\infty} \frac{A^{i-1}x^i}{i!}$, $\Phi \triangleq e^{Ah}$, and*

$$\mathcal{O}_{x,k} \triangleq \int_{t_k}^{t_{k+1}} \phi(t_{k+1} - s) B_f \frac{d}{ds}\Big(f(x(s), \omega(s))\Big)\, ds,$$
$$\mathcal{O}_{f,k} \triangleq \int_{t_k}^{t_{k+1}} \frac{d}{ds}\Big(f(x(s), \omega(s))\Big)\, ds. \tag{3}$$

*Proof.* Refer to Appendix A. □

Prop. 1 gives a discretized version of classical procedure of extending the state with the disturbance and leaving the disturbance derivative as the new uncertain system input. However, in the discrete case, the new uncertain inputs appear in the integral forms $\mathcal{O}_{x,k}$ and $\mathcal{O}_{f,k}$ –although they still depending on the disturbance derivative and, consequently, they are null for constant disturbances.

Finally, the next assumption is considered for the observer design as it assures the observability of (2):

**Assumption 4.** [21] The triplet $(\Phi, \Gamma_1, C)$ is observable and $\text{rank}\begin{pmatrix}\begin{bmatrix}\Phi - I_n & \Gamma_2 \\ -C & 0\end{bmatrix}\end{pmatrix} = n + q$.

**Remark 1.** Observability of the triplet $(A, B_u, C)$ does not necessarily imply observability of $(\Phi, \Gamma_1, C)$. The observability may be lost due to undesired zero-pole cancellations [22].

## 3. Predictive ESO-based controller

This section develops the predictive ESO-based controller. To this purpose a discrete-time ESO is firstly considered in order to get estimates of $x(t_k)$ and $f(x(t_k), \omega(t_k))$ in terms of the available measurements, $y(t_k)$. Then, the estimates are employed to compute a sequence of future state-predictions –under the assumption that the disturbances remain constant over the prediction-horizon– and, finally, the control action is defined as the signal minimizing a constrained quadratic-cost penalizing deviations in the state-predictions from zero.

*A discrete-time ESO*

Based on (2), the following discrete ESO is considered:

$$\hat{x}_{k+1} = \Phi \hat{x}_k + \Gamma_1 u_k + \Gamma_2 \hat{f}_k + L_x(y(t_k) - C\hat{x}_k), \tag{4a}$$
$$\hat{f}_{k+1} = \hat{f}_k + L_f(y(t_k) - C\hat{x}_k), \tag{4b}$$

where $\hat{x}_k$ and $\hat{f}_k$ are estimates of $x(t_k)$ and $f(x(t_k),\omega(t_k))$, respectively; while $L_x$ and $L_f$ are design matrices of appropriate dimensions.

The observer (4) can be seen as a discretized version of the generalized ESO [17] or, similarly, as a particular structure of the Proportional Integral Observer (PIO) [21].

*State-predictions and control sequence*

Let $N \in \mathbb{N}$ be the prediction horizon. Consider a sequence of control actions $\mathbf{u}_k \triangleq [u_{k|k}^T\ u_{k+1|k}^T\ ...\ u_{k+N-1|k}^T]^T$, with $u_{k|k} \triangleq u_k$; and a sequence of future state-predictions, $\mathbf{x}_k \triangleq [\hat{x}_{k|k}^T,\ \hat{x}_{k+1|k}^T,\ ...,\ \hat{x}_{k+N|k}^T]^T$, with $\hat{x}_{k|k} \triangleq \hat{x}_k$. The notation $\hat{x}_{k+j|k}$ denotes a prediction of $x(t_{k+j})$ that is made with the available observations at $t = t_k$.

The state-predictions are computed by:

$$\hat{x}_{k+j+1|k} = \Phi\hat{x}_{k+j|k} + \Gamma_1 u_{k+j|k} + \Gamma_2\hat{f}_k, \quad 0 \le j \le N-1. \tag{5}$$

Note that, under perfect observation conditions –i.e. $\hat{x}_k = x(t_k)$, $\hat{f}_k = f(x(t_k),\omega(t_k))$– the future-states are predicted by neglecting the residual terms $\mathcal{O}_{x,k}$ and $\mathcal{O}_{f,k}$ in (2). This is equivalent to say that the disturbance will remain constant over the whole prediction-horizon; which can be interpreted as an strengthen version of the implicit assumption of null-disturbance derivative that is taken for the ESO design [17, 23, 18].

*Predictive controller*

Based on (4)-(5), the following performance cost-index is considered:

$$V_N(\hat{x}_k,\hat{f}_k,\mathbf{u}_k) \triangleq \sum_{j=0}^{N-1}\Big[||\hat{x}_{k+j|k}||_Q^2 + ||u_{k+j|k} + \Gamma_1^\dagger\Gamma_2\hat{f}_k||_R^2\Big] + ||\hat{x}_{k+N|k}||_P^2, \tag{6}$$

where $Q \in \mathbb{R}^{n\times n}$ and $R \in \mathbb{R}^{m\times m}$ are positive definite weighting matrices; and $0 \prec P \in \mathbb{R}^{n\times n}$ is defined such that $\Phi^T P\Phi - P + Q = 0$.

The control action is then generated by:

$$u_k = K\mathbf{u}_k^*, \tag{7}$$

being $K \triangleq [I_m,\ 0_{m,\,m\cdot(N-1)}]$ and

$$\mathbf{u}_k^* = \arg\min_{\mathbf{u}_k}\ V_N(\hat{x}_k,\hat{f}_k,\mathbf{u}_k) \tag{8a}$$

$$\text{s.t. Eq. (5)} \tag{8b}$$

$$u_{min} \le u_{k+j|k} \le u_{max}, \tag{8c}$$

Eqs. (7)-(8) represent the proposed predictive ESOBC with guaranteed stability. As $V_N(\cdot)$ is a quadratic-cost, problem (8) has always a feasible solution if $u_{max} > u_{min}$.

The main differences with respect to other predictive ESOBC are two elements in the cost (6): **i)** the fixed-terminal cost, $||\hat{x}_{k+N|k}||_P^2$, and **ii)** the disturbance-compensation term, $\Gamma_1^\dagger\Gamma_2\hat{f}_k$.

Both elements play a key role in the closed-loop properties of the resulting controller. The fixed-terminal cost needs to be included in order to guarantee its closed-loop stability [24]. It permits to deal with some technical difficulties that arise due to the finite-horizon nature of $V_N(\cdot)$ –more details on this are given in Sec. 4. The disturbance compensation term is introduced in order to penalize deviations of the control action from $\Gamma_1^\dagger\Gamma_2\hat{f}_k$; which is regarded as the optimal value to compensate for the matched part of $\hat{f}_k$. This term endows to the controller with the property of rejecting constant matched disturbances.

## 4. Closed-loop stability

This section analyzes the closed-loop stability of the proposed predictive ESOBC.

The main result is to prove that –for matched disturbances– the state $x(t_k)$ will be driven by (7)-(8) to a bounded region around the origin whose size exclusively depends on the observation errors of (4). This is the same behavior that is normally required for non-predictive ESOBCs. The result is proved by using the optimal cost, $V_N(\hat{x}_k,\hat{f}_k,\mathbf{u}_k^*)$, as a Lyapunov function; which is possible thanks to the insertion of $||\hat{x}_{k+N|k}||_P^2$ and $\Gamma_1^\dagger\Gamma_2\hat{f}_k$ in (6).

To this end, the properties of observation-error resulting from (2), (4), are firstly analyzed:

*Input-to-State Stability of the observation error*

Let us define the augmented states:

$$\eta_k \triangleq [x(t_k)^T,\ f(x(t_k),\omega(t_k))^T]^T,$$
$$\hat{\eta}_k \triangleq [\hat{x}_k^T,\ \hat{f}_k^T]^T,$$
$$\mathcal{O}_k^T \triangleq [\mathcal{O}_{x,k}^T, \mathcal{O}_{f,k}^T]^T.$$

By subtracting (4) from (2), the observation error, $\tilde{\eta}_k \triangleq \eta_k - \hat{\eta}_k$, satisfies:

$$\tilde{\eta}_{k+1} = (M - LG)\,\tilde{\eta}_k + \mathcal{O}_k, \tag{9}$$

being $M \triangleq \begin{bmatrix}\Phi & \Gamma_2\\ 0 & I_q\end{bmatrix}$; $G \triangleq \begin{bmatrix}C & 0\end{bmatrix}$; $L \triangleq \begin{bmatrix}L_x^T & L_f^T\end{bmatrix}^T$.

The following lemma establish the ISS of (9):

**Lemma 1.** *Under Asm. 1-4. Let $L_x, L_f$ be matrices such that $M - LG$ has its eigenvalues inside the unit circle. Then, there exist a class $\mathcal{KL}$-function, $\beta_1(\cdot,\cdot)$, a class $\mathcal{K}$-function, $\gamma_1(\cdot)$, a bounded constant, $\mu \triangleq h\sqrt{\|\phi(h)B_f\|^2+1}$, and a bounded sequence, $\chi_k \triangleq \sup_{s\in[t_k,t_{k+1}]}\{\|\dot{x}(s)\|\}$; such that, for each initial state $\tilde{\eta}_0$, the observation error satisfies that:*

$$\|\tilde{\eta}_k\| \le \beta_1\big(\|\tilde{\eta}_0\|,t_k\big) + \gamma_1\big(\mu(\epsilon_{dx}\|\chi_{[0,k-1]}\|_\infty + \epsilon_{d\omega}\epsilon_{\dot{\omega}})\big);$$

*Proof.* Asm. 4 guarantees the existence of $L_x$, $L_f$ such that $(M-LG)$ has its eigenvalues inside the unit circle [21]. Let $L_x$, $L_f$ be some matrices satisfying it; then there exist a

class $\mathcal{KL}$-function, $\beta_1(\cdot,\cdot)$, and a class $\mathcal{K}$-function, $\gamma_1(\cdot)$, such that [25]:

$$\|\tilde{\eta}_k\| \leq \beta_1(\|\tilde{\eta}_0\|, t_k) + \gamma_1(\|\mathcal{O}_{[0,k-1]}\|_\infty). \tag{10}$$

By taking norms in (3), expressing $\frac{\mathrm{d}}{\mathrm{d}s} f(x(s),\omega(s))$ in terms of its partial derivatives and applying the bounds in Asm. 1; we have:

$$\|\mathcal{O}_{x,k}\| \leq \bar{\mu}(\epsilon_{dx}\chi_k + \epsilon_{d\omega}\epsilon_{\dot{\omega}})h,$$
$$\|\mathcal{O}_{f,k}\| \leq (\epsilon_{dx}\chi_k + \epsilon_{d\omega}\epsilon_{\dot{\omega}})h,$$

with $\bar{\mu} \triangleq \sup_{s\in[t_k,t_{k+1}]}\{\|\phi(t_{k+1}-s)B_f\|\} = \|\phi(h)B_f\|,\ \forall\, k$.

The proof follows by doing:

$$\|\mathcal{O}_k\| = \sqrt{\|\mathcal{O}_{x,k}\|^2 + \|\mathcal{O}_{f,k}\|^2} \leq (\epsilon_{dx}\chi_k + \epsilon_{d\omega}\epsilon_{\dot{\omega}})\mu,$$

with $\mu \triangleq h\sqrt{\bar{\mu}^2+1}$; and substituting it into (10). □

Lemma 1 illustrates some qualitative properties of the observation-error behavior that are insightful. For constant disturbances, i.e. $(\epsilon_{dx}\|\chi_{[0,k-1]}\|_\infty + \epsilon_{d\omega}\epsilon_{\dot{\omega}}) = 0$, the observation-error is bounded by $\|\tilde{\eta}_k\| \leq \beta_1(\|\tilde{\eta}_0\|, t_k)$; indicating that it goes to zero as $k \to \infty$. This is the same property that actually holds for the continuous-time case.

For non-constant disturbances, the following ultimate bound holds: $\|\tilde{\eta}_k\| \leq \gamma_1\big(\mu(\epsilon_{dx}\|\chi_{[0,k-1]}\|_\infty + \epsilon_{d\omega}\epsilon_{\dot{\omega}})\big)$; indicating that the observation-error may increase with respect to $(\epsilon_{dx}\|\chi_{[0,k-1]}\|_\infty + \epsilon_{d\omega}\epsilon_{\dot{\omega}})$ –i.e. the rate of variation of the disturbance– or with respect to $\mu$ –i.e. the discretization period.

*Input-to-State Stability of the predictive ESOBC*

The following theorem establish the ISS of the resulting closed-loop formed by (7)-(8) and (1).

**Theorem 1.** *Under Asm. 1-4. Consider that* $\Gamma_2 = \alpha\Gamma_1$, $\alpha \in \mathbb{R}$, *and that* $u_{min} \leq -\alpha\hat{f}_k \leq u_{max},\ \forall\, k$. *Then, the closed-loop formed by* (7)-(8) *and* (1) *satisfies that:*

$$||x(t_k)|| \leq \beta_2(||x_0||, k) + \gamma_2(||\tilde{\eta}_{[0,k-1]}||).$$

*being* $\beta_2(\cdot,\cdot)$ *a class* $\mathcal{KL}$*-function;* $\gamma_2(\cdot)$ *a class* $\mathcal{K}_\infty$*-function; and* $\tilde{\eta}_k \triangleq \eta(t_k) - \hat{\eta}_k$.

*Proof.* Let us consider $V_N(\hat{x}_k, \hat{f}_k, \boldsymbol{u}_k^*)$ –with $V_N(\cdot)$ given by (6) and $\boldsymbol{u}_k^*$ resulting by solving (8)– as a Lyapunov function. Then, the following inequalities hold:

$$\|\hat{x}_k\|_Q^2 \leq V_N(\hat{x}_k, \hat{f}_k, \boldsymbol{u}_k^*) \leq c\|\hat{x}_k\|^2, \tag{11}$$
$$V_N(\hat{x}_{k+1}, \hat{f}_{k+1}, \boldsymbol{u}_{k+1}^*) - V_N(\hat{x}_k, \hat{f}_k, \boldsymbol{u}_k^*) \leq \tag{12}$$
$$- ||\hat{x}_k||_Q^2 + \Psi(||\tilde{y}_k||),$$

being $c > 0$, $\tilde{y}_k \triangleq y(t_k) - C\hat{x}_k$, and $\Psi(\cdot)$ a class $\mathcal{K}_\infty$-function.

Inequality (11) is proved in Appendix B.1, while (12) is proved in Appendix B.1.

This implies that there exist a $\mathcal{KL}$-function, $\bar{\beta}_2(\cdot,\cdot)$, and a class $\mathcal{K}$-function, $\bar{\alpha}_2(\cdot)$ such that [25]:

$$||\hat{x}_k|| \leq \bar{\beta}_2(||\hat{x}_0||, k) + \bar{\alpha}_2(||\tilde{y}_{[0,k-1]}||_\infty). \tag{13}$$

The rest of the prove follows by considering the observation error definition:

$$\|x(t_k)\| \leq \|\hat{x}_k\| + \|\tilde{x}_k\| \leq \|\hat{x}_k\| + \|\tilde{\eta}_k\|$$

where, by (13),

$$\begin{aligned}
\|x(t_k)\| &\leq \bar{\beta}_2(||\hat{x}_0||, k) + \bar{\alpha}_2(||\tilde{y}_{[0,k-1]}||_\infty) + \|\tilde{\eta}_k\|,\\
&\leq \bar{\beta}_2(||x_0 - \tilde{x}_0||, k) + \bar{\alpha}_2(||\tilde{\eta}_{[0,k-1]}||_\infty||) + ||\tilde{\eta}_k||,\\
&\leq \bar{\beta}_2(2\max(||x_0||, ||\tilde{x}_0||), k) + \bar{\alpha}_2(||\tilde{\eta}_{[0,k-1]}||) + ||\tilde{\eta}_k||,\\
&\leq \bar{\beta}_2(2||x_0||, k||) + \bar{\beta}_2(2||\tilde{x}_0||, 0) + \bar{\alpha}_2(||\tilde{\eta}_{[0,k-1]}||) + ||\tilde{\eta}_k||,\\
&\leq \beta_2(||x_0||, k) + \alpha_2(||\tilde{\eta}_{[0,k-1]}||);
\end{aligned}$$

which completes de proof. □

By Theorem 1, it is seen that the ultimate bound of $x(t_k)$ depends on the observation error; which was the desired property. By Lemma 1, the observation-error depends on the rate of variation of $f(x(t),\omega(t))$ and on the discretization period; being null for constant disturbances. Thus, this predictive controller achieves asymptotic convergence for constant matched disturbances.

## 5. Comparisons with the Generalized ESOBC

This section is introduced in order to illustrate how this predictive ESOBC relates with the Generalized ESOBC [17] in the case of no actuator constraints.

Let us substitute (5) into (6), and after some algebraic manipulation, problem (8) can be expressed as:

$$\begin{aligned}
\mathbf{u}_k^* = \arg\min_{\mathbf{u}_k}\ & \mathbf{u}_k^T H \mathbf{u}_k + c(\hat{x}_k, \hat{f}_k)^T \mathbf{u}_k\\
\text{s.t. } & \mathcal{I}_m u_{min} \leq \mathbf{u}_k \leq \mathcal{I}_m u_{max},
\end{aligned} \tag{14}$$

with $c(\hat{x}_k, \hat{f}_k) \triangleq 2\big[\Upsilon_1^T\mathcal{Q}\Pi\hat{x}_k + \Upsilon_1^T\mathcal{Q}\Upsilon_2\hat{f}_k + \mathcal{R}^T\mathcal{I}_m\Gamma_1^\dagger\Gamma_2\hat{f}_k\big]$ and $H \triangleq \Upsilon_1^T\mathcal{Q}\Upsilon_1 + \mathcal{R}$; being

$$\Pi \triangleq \begin{bmatrix} I_n \\ \Phi \\ \Phi^2 \\ \vdots \\ \Phi^N \end{bmatrix}, \qquad \Upsilon_1 \triangleq \begin{bmatrix} 0 & 0 & ... & 0 \\ \Gamma_1 & 0 & ... & 0 \\ \Phi\Gamma_1 & \Gamma_1 & ... & 0 \\ \vdots & \vdots & \ddots & \vdots \\ \Phi^{N-1}\Gamma_1 & \Phi^{N-2}\Gamma_1 & ... & \Gamma_1 \end{bmatrix},$$

$$\Upsilon_2 \triangleq \begin{bmatrix} 0 \\ \Gamma_2 \\ (\Phi+I)\Gamma_2 \\ \vdots \\ (\Phi^{N-1}+\ldots\Phi+I)\Gamma_2 \end{bmatrix}, \quad \mathcal{R} \triangleq \begin{bmatrix} R & 0 & ... & 0 \\ 0 & R & ... & 0 \\ \vdots & \vdots & \ddots & \vdots \\ 0 & 0 & ... & R \end{bmatrix},$$

| Param. | Value | Quantifies |
|---|---|---|
| $\tau_1$ | 49 ($\text{min}^{-1}$) | Delay in absorption |
| $\tau_2$ | 47 ($\text{min}^{-1}$) | Delay in absorption |
| $C_l$ | 2010 (ml/min) | Insulin clearance |
| $p_2$ | 1.06e-2 ($\text{min}^{-1}$) | Delay in insulin action |
| $S_I$ | 8.11e-4 (ml/$\mu$U) | Insulin sensitivity |
| $k_{gezi}$ | 2.20e-3 ($\text{min}^{-1}$) | Effect of glucose to reduce glucose itself |
| $k_{egp}$ | 1.33 (mg/dl/min) | Glucose production rate |

Table 1: Parameters in (17). Numerical values corresponding to the ones identified for Patient 1 in [26].

$$\mathcal{Q} \triangleq \begin{bmatrix} Q & 0 & ... & 0 & 0 \\ 0 & Q & ... & 0 & 0 \\ \vdots & \vdots & \ddots & \vdots & \vdots \\ 0 & 0 & ... & Q & 0 \\ 0 & 0 & ... & 0 & P \end{bmatrix}, \qquad \mathcal{I}_m \triangleq \begin{bmatrix} I_m \\ I_m \\ \vdots \\ I_m \end{bmatrix}.$$

with $\mathcal{I}_m \in \mathbb{R}^{m\cdot N\times m}$, $\Pi \in \mathbb{R}^{n\cdot(N+1)\times n}$, $\Upsilon_1 \in \mathbb{R}^{n(N+1)\times mN}$, $\Upsilon_2 \in \mathbb{R}^{n(N+1)\times r}$, $\mathcal{R} \in \mathbb{R}^{m\cdot N\times m\cdot N}$, $\mathcal{Q} \in \mathbb{R}^{n\cdot(N+1)\times n\cdot(N+1)}$.

If there is no active saturations –i.e. $u_{max} = +\infty$, $u_{min} = -\infty$; then, the solution of (14) is given by:

$$\left.\frac{\partial\big(\mathbf{u}_k^T H\mathbf{u}_k + c(\hat{x}_k,\hat{f}_k)^T\mathbf{u}_k\big)}{\partial\mathbf{u}_k}\right|_{\mathbf{u}_k} = H\mathbf{u}_k^* + c(\hat{x}_k,\hat{f}_k) = 0$$

which, by (7), results in:

$$u_k = K_x\hat{x}_k + K_f\hat{f}_k, \tag{15}$$

with

$$\begin{aligned} K_x &\triangleq -KH^{-1}\Upsilon_1^T\mathcal{Q}\Pi, \\ K_f &\triangleq -KH^{-1}(\Upsilon_1^T\mathcal{Q}\Upsilon_2 + \mathcal{R}^T\mathcal{I}_m\Gamma_1^\dagger\Gamma_2), \end{aligned} \tag{16}$$

which corresponds to a discretized version of the GESOBC presented in [17]; but with different gains given by $Q$, $R$.

## 6. Simulation study

This section introduces an illustrative example to highlight the advantages of this control approach. To this end, a simulation for closed-loop glucose control in patients with type-1 diabetes has been considered; a recently popular control problem that involves strong actuator saturations and disturbances.

*Glucose-Insulin model for patients with type-1 diabetes.*

Let us consider the following system [27, 26, 28]:

$$\begin{aligned} \dot{x}_1(t) &= -\frac{1}{\tau_1}x_1(t) + \frac{1}{\tau_1 C_l}u(t), \\ \dot{x}_2(t) &= \frac{1}{\tau_2}x_1(t) - \frac{1}{\tau_2}x_2(t), \\ \dot{x}_3(t) &= p_2 S_I\, x_2(t) - p_2\, x_3(t), \\ \dot{x}_4(t) &= -k_{gezi}x_4(t) - x_3(t)x_4(t) + k_{egp} + d(t), \\ y(t_k) &= x_4(t_k), \end{aligned} \tag{17}$$

where $u(t)$ represents the insulin delivery at Sub-Cutaneous (SC) level, $x_1(t)$ is the insulin concentration at SC level, $x_2(t)$ is the plasma insulin concentration, $x_3(t)$ is the insulin effect, $x_4(t)$ is the Gucose Concentration (GC) and $d(t)$ represents the glucose appearance following a meal. The rest of the parameters are defined in Table 1.

System (17) is a clinically identified model that represents –for a given person– how the GC in blood, $x_4(t)$, is affected by: **i)** insulin deliveries at sub-cutaneous level, i.e. $u(t)$; and **ii)** meals that the person takes, i.e. $d(t)$, which have the following form [26]:

$$d(t) = \frac{C_H(t)}{V_G\tau_m^2}t\text{e}^{-\frac{t}{\tau_m}}, \tag{18}$$

where $C_H$ represents the amount of consumed carbohydrates, while $V_G = 253$ and $\tau_m = 47$ are the identified parameters for Patient 1 in [26].

*Control objective and limitations*

The main objective is to design a controller that automatically injects insulin, $u(t)$, in response to unannounced/unknown meals that the person takes, $d(t)$.

The objective is to keep the GC at $x_4^* = 100$ (mg/dl). In no case can be higher than 250 (mg/dl) or lower than 54 (mg/dl) as it may lead to severe hyperglycemia or hypoglycemia, respectively. After a meal, optimal values should range between $70\,(\text{mg/dl}) < x_4(t) < 180\,(\text{mg/dl})$.

The main limitations for the controller are: **i)** $u(t) \geq 0$, i.e. insulin can be injected but not subtracted; **ii)** $d(t)$ is unknown for the controller, i.e. the controller does not have information about when and how much the patient eats; **iii)** there are only discrete measures of $x_4(t)$ with period $T = 5$ min.

*Comparative simulations*

Fig. 1 contains a comparative simulation of a 24h-day in closed-loop glucose control. Concretely, a scenario where the patient consumes 50g of Carbohydrates (CHO) at 8h, 70g CHO at 13h, 100g CHO at 19h, and 30g CHO at 22h; has been simulated –which are standard values for consumed CHO [28].

The continous line represents the simulation result with the proposed predictive ESOBC (7)-(8). It has been designed with a linearized version of (17) around the nominal operating point $u^* = 22750\,\mu U/min$, $x_1^* = x_2^* = 13.670$, $x_3^* = 0.011$, $x_4^* = 100$; which is given by:

$$\begin{aligned} \dot{\tilde{x}}(t) &= A\tilde{x}(t) + B_u\tilde{u}(t) + B_f f(\tilde{x}, d(t)), \\ y(t_k) &= C\tilde{x}(t_k), \end{aligned}$$

where $f(\tilde{x}, d(t)) \triangleq \mathcal{O}_l(\tilde{x}) + d(t)$, being $\mathcal{O}_l(\tilde{x})$ the lineariza-

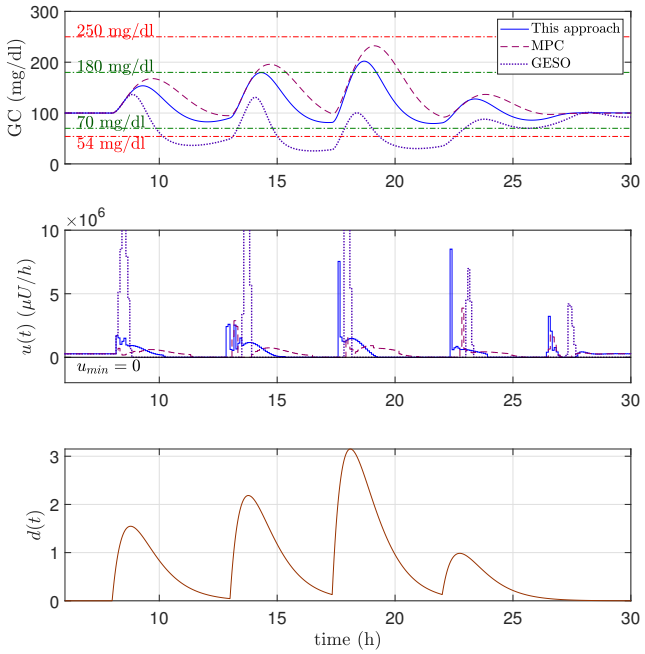


Figure 1: Comparative simulation results.

tion residues; $\tilde{x}(t) \triangleq x(t) - x^*$, $\tilde{u}(t) \triangleq u(t) - u^*$ and

$$A = \begin{bmatrix} -1/\tau_1 & 0 & 0 & 0 \\ 1/\tau_2 & -1/\tau_2 & 0 & 0 \\ 0 & p_2 S_I & -p_2 & 0 \\ 0 & 0 & -x_4^* & -x_3^* - k_{gezi} \end{bmatrix},$$

$$B_u = \begin{bmatrix} 1/(\tau_1 C_l) & 0 & 0 & 0 \end{bmatrix}^T,$$

$$B_f = \begin{bmatrix} 0 & 0 & 0 & 1 \end{bmatrix}^T,$$

$$C = \begin{bmatrix} 0 & 0 & 0 & 1 \end{bmatrix}.$$

The rest of the controller parameters are: $\tilde{u}_{min} = -u^*$; $\bar{u}_{max} = +\infty$; $N = 18$ (prediction-horizon of 90 min); $Q = \begin{bmatrix} I_3 & 0 \\ 0 & 100 \end{bmatrix}$; $R = 1$; and observer gains $L_x = [0.0003, 0.0032, 0.0001, 0.3518]^T$, $L_f = 0.0167$.

The dashed line represents the simulation result with a standard Model Predictive Control (MPC) strategy. For fair comparison, the same cost-index (6) and observer (4) have been employed. The main difference is that the matrix $\Gamma_2$, in (5)-(6) has been set to zero. In this sense, the disturbance estimate is not employed in the computed predictions. This is the main difference between predictive ESOBC and conventional MPC strategies.

The dotted line represents the system performance with the GESOBC approach [17]. For fair comparison, the gains have been computed according to (16). The main difference in this case is that the GESOBC does not consider the actuator saturations in the computed control signal.

From the simulation results, it can be seen that the predictive ESOBC produces a relatively natural control-behavior: it injects an insulin bolus at the same time that the meal-disturbance appears. This is because the meal-disturbance is detected by (4) and its effect in the GC is predicted in (5). It closely resembles to the control that manually carries out a diabetic person; who manually injects an insulin bolus into his body before each meal.

However, this performance is not achieved by the other two strategies. The MPC approach does not injects the peak of insulin at the beginning of each meal and, as a consequence, the GC significantly augments afterwards. This happens because the effect of the meal-disturbance in the GC is not considered in the computed predictions; consequently, the controller is not evaluating if the person has eaten something and the effects that it may have in the GC.

On the other hand, GESOBC detects the meal and automatically injects insulin. However, as it is not considering that the insulin cannot be latterly extracted from the body –i.e. the actuator limitations– it injects an excessive amount of insulin; driving the patient to hypoglycemia.

*Simulation details and computation time*

The simulations have been performed with MATLAB® R2019a in a computer running Windows 10 with a processor Intel(R) Core(TM) i7-6700HQ 2.6GHz. The optimization (8) has been performed with the `quadprog()` function of the Optimization toolbox.

The required computation time for solving (8) is of the order of milliseconds. In particular, for 360 control iterations, the computation time has had a mean value of 4.9 ms, with a standard deviation of 1.9 ms, a maximum value of 9.8 ms and a minimum value of 2.2 ms.

## 7. Conclusions

This paper has developed a predictive ESO-based discrete controller with guaranteed stability for complex uncertain constrained systems.

The controller is constructed with a discrete ESO and a quadratic-cost predictive controller that includes two fixed elements –i.e. a fixed terminal cost and a disturbance compensation term. With this formulation, it is proved the resulting closed-loop is input-to-state stable, with the same qualitative properties that conventional ESO-based controllers and the advantage of constraints handling.

Some relationships of this predictive ESOBC with respect to the Generalized ESOBC has been highlighted. A simulation study of closed-loop glucose control has been included in order to compare this control approach against conventional predictive controllers and non-predictive ESOBC; showing that it offers better performance and maintains the process and control variables in the desired ranges.

## Acknowledgment

This work was partially supported by projects FPU15/02008 and TIN2017-86520-C3-1-AR, Ministerio de Economia y Competitividad, Spain.

Tito L.M Santos and Julio Elias Normey-Rico would also like to thank CNPq project 305785/2015-0 for its financial support.

## References


[1] W. H. Chen, J. Yang, L. Guo, S. Li, Disturbance–observer–based control and related methods—An overview, IEEE Transactions on Industrial Electronics 63 (2) (2016) 1083–1095.

[2] L.-L. Xie, L. Guo, How much uncertainty can be dealt with by feedback?, IEEE Transactions on Automatic Control 45 (12) (2000) 2203–2217.

[3] Z. Zhu, D. Xu, J. Liu, Y. Xia, Missile guidance law based on extended state observer, IEEE Transactions on Industrial Electronics 60 (12) (2012) 5882–5891.

[4] S. E. Talole, J. P. Kolhe, S. B. Phadke, Extended-state-observer-based control of flexible-joint system with experimental validation, IEEE Transactions on Industrial Electronics 57 (4) (2009) 1411–1419.

[5] J. Yao, Z. Jiao, D. Ma, Adaptive robust control of DC motors with extended state observer, IEEE transactions on industrial electronics 61 (7) (2013) 3630–3637.

[6] J. Yao, Z. Jiao, D. Ma, Extended-state-observer-based output feedback nonlinear robust control of hydraulic systems with backstepping, IEEE Transactions on Industrial Electronics 61 (11) (2014) 6285–6293.

[7] L. Dong, Y. Zhang, Z. Gao, A robust decentralized load frequency controller for interconnected power systems, ISA transactions 51 (3) (2012) 410–419.

[8] A. Castillo, P. García, R. Sanz, P. Albertos, Enhanced extended state observer-based control for systems with mismatched uncertainties and disturbances, ISA transactions 73 (2018) 1–10.

[9] C. Liu, R. R. Negenborn, H. Zheng, X. Chu, A state-compensation extended state observer for model predictive control, European Journal of Control 36 (2017) 1 – 9.

[10] A. Liu, W.-A. Zhang, L. Yu, H. Yan, R. Zhang, Formation control of multiple mobile robots incorporating an extended state observer and distributed model predictive approach, IEEE Transactions on Systems, Man, and Cybernetics: Systems (2018).

[11] F. Zhang, X. Wu, J. Shen, Extended state observer based fuzzy model predictive control for ultra-supercritical boiler-turbine unit, Applied Thermal Engineering 118 (2017) 90–100.

[12] B. Panchal, S. Talole, Generalized ESO and predictive control based robust autopilot design, Journal of Control Science and Engineering (2016).

[13] Z.-y. Song, G.-f. Yan, D.-j. Zhao, ESO-based robust predictive control of lunar module with fuel sloshing dynamics, Journal of Central South University 24 (3) (2017) 589–598.

[14] D. Ma, Y. Xia, T. Li, K. Chang, Active disturbance rejection and predictive control strategy for a quadrotor helicopter, IET Control Theory & Applications 10 (17) (2016) 2213–2222.

[15] M. Yue, C. An, Z. Li, Constrained adaptive robust trajectory tracking for wip vehicles using model predictive control and extended state observer, IEEE Transactions on Systems, Man, and Cybernetics: Systems 48 (5) (2016) 733–742.

[16] H. Liu, S. Li, Speed control for PMSM servo system using predictive functional control and extended state observer, IEEE Transactions on Industrial Electronics 59 (2) (2011) 1171–1183.

[17] S. Li, J. Yang, W. H. Chen, X. Chen, Generalized extended state observer based control for systems with mismatched uncertainties, IEEE Transactions on Industrial Electronics 59 (12) (2012) 4792–4802.

[18] Y. Huang, W. Xue, Active disturbance rejection control: methodology and theoretical analysis, ISA transactions 53 (4) (2014) 963–976.

[19] B.-Z. Guo, Z.-l. Zhao, On the convergence of an extended state observer for nonlinear systems with uncertainty, Systems & Control Letters 60 (6) (2011) 420–430.

[20] A. Castillo, P. García, E. Fridman, P. Albertos, Extended state observer-based control for systems with locally lipschitz uncertainties: Lmi-based stability conditions, Systems & Control Letters 134 (2019) 104526.

[21] J.-L. Chang, Applying discrete-time proportional integral observers for state and disturbance estimations, IEEE Transactions on Automatic Control 51 (5) (2006) 814–818.

[22] K. J. Åström, B. Wittenmark, Computer-controlled systems: theory and design, Prentice Hall, 1997.

[23] J. Han, From PID to active disturbance rejection control, IEEE transactions on Industrial Electronics 56 (3) (2009) 900–906.

[24] D. Q. Mayne, J. B. Rawlings, C. V. Rao, P. O. Scokaert, Constrained model predictive control: Stability and optimality, Automatica 36 (6) (2000) 789–814.

[25] Z.-P. Jiang, Y. Wang, Input-to-state stability for discrete-time nonlinear systems, Automatica 37 (6) (2001) 857–869.

[26] S. S. Kanderian, S. Weinzimer, G. Voskanyan, G. M. Steil, Identification of intraday metabolic profiles during closed-loop glucose control in individuals with type 1 diabetes (2009).

[27] D. Stocker, S. Kanderian, G. Cortina, T. Nitzan, J. Plummer, G. Steil, J. Mastrototaro, Virtual patient software system for educating and treating individuals with diabetes (2006).

[28] S. S. Kanderian, S. A. Weinzimer, G. M. Steil, The identifiable virtual patient model: comparison of simulation and clinical closed-loop study results, Journal of diabetes science and technology 6 (2) (2012) 371–379.


## Appendix A. Proof of Proposition 1

Integration of (1) leads to:

$$x(t_{k+1}) = e^{Ah}x(t_k) + \int_{t_k}^{t_{k+1}} e^{A(t_{k+1}-s)}B_u u(s)\mathrm{ds} + \\ + \int_{t_k}^{t_{k+1}} e^{A(t_{k+1}-s)}B_f f(x(s),\omega(s))\mathrm{ds},$$

where, by applying Assumption 3 and noting that $\int_{t_k}^{t_{k+1}} e^{A(t_{k+1}-s)}\mathrm{ds} = \sum_{i=1}^{\infty} \frac{A^{i-1}h^i}{i!} \triangleq \phi(h)$, results in:

$$x(t_{k+1}) = e^{Ah}x(t_k) \quad + \quad \phi(h)B_u u_k \quad + \\ + \int_{t_k}^{t_{k+1}} e^{A(t_{k+1}-s)}B_f f(x(s),\omega(s))\mathrm{ds}. \tag{A.1}$$

On the other hand, by Taylor theorem, the uncertainty at $t_{k+1}$ is given by:

$$f(x(t_{k+1}),\omega(t_{k+1})) = \\ = f(x(t_k),\omega(t_k)) + \int_{t_k}^{t_{k+1}} \frac{\mathrm{d}}{\mathrm{ds}}\Big(f(x(s),\omega(s))\Big)\mathrm{ds}. \tag{A.2}$$

Now, integrating by parts the integral in (A.1) leads to:

$$\int_{t_k}^{t_{k+1}} e^{A(t_{k+1}-s)}B_f f(x(s),\omega(s))\mathrm{ds} = \\ - A^{-1}B_f f(x(t_{k+1}),\omega(t_{k+1})) + A^{-1}e^{Ah}B_f f(x(t_k),\omega(t_k)) + \\ + \int_{t_k}^{t_{k+1}} A^{-1}e^{A(t_{k+1}-s)}B_f \frac{\mathrm{d}}{\mathrm{ds}}\Big(f(x(s),\omega(s))\Big)\mathrm{ds},$$

where, by substituting (A.2), gives:

$$\int_{t_k}^{t_{k+1}} e^{A(t_{k+1}-s)}B_f f(x(s),\omega(s))\mathrm{ds} = \phi(h)B_f f(x(t_k),\omega(t_k)) + \int_{t_k}^{t_{k+1}} \underbrace{A^{-1}\left(e^{A(t_{k+1}-s)}-I_n\right)}_{=\phi(t_{k+1}-s)} B_f \frac{\mathrm{d}}{\mathrm{ds}}\Big(f(x(s),\omega(s))\Big)\mathrm{ds}.$$

The proof follows by substituting the above expression into (A.1).

## Appendix B. Proof of Theorem 1

*Appendix B.1. Proof of inequality* (11)

The lower bound follows by the definition of $V_N(\cdot)$:

$$V_N(\hat{x}_k,\hat{f}_k,\boldsymbol{u}_k) = ||\hat{x}_k||_Q^2+||\hat{x}_{k+1|k}||_Q^2+\ldots+||\hat{x}_{k+N-1|k}||_Q^2 + \sum_{j=0}^{N-1}\left[||u_{k+j|k}+\alpha\hat{f}_k||_R^2\right]+||\hat{x}_{k+N|k}||_P^2; \quad \text{(B.1)}$$

which, clearly, satisfies $||\hat{x}_k||_Q^2 \leq V_N(\cdot,\cdot,\boldsymbol{u}_k)$ for any $\boldsymbol{u}_k$.

In order to prove de upper bound, consider the control sequence $\boldsymbol{u}_k^c = [-\alpha\hat{f}_k^T, -\alpha\hat{f}_k^T, ..., -\alpha\hat{f}_k^T]^T$. Then, the cost (B.1) becomes:

$$V_N(\hat{x}_k,\hat{f}_k,\boldsymbol{u}_k^c) = ||\hat{x}_k||_Q^2+||\hat{x}_{k+1|k}||_Q^2+\ldots+||\hat{x}_{k+N-1|k}||_Q^2 + ||\hat{x}_{k+N|k}||_P^2; \quad \text{(B.2)}$$

and, by (5), it holds that $\hat{x}_{k+j|k} = \Phi^j\hat{x}_k$ –where the matched condition, $\Gamma_1 = \alpha\Gamma_2$, and the control sequence, $u_{k+j|k} = u^c_{k+j|k} = -\alpha\hat{f}_k$ have been substituted. Hence:

$$V_N(\hat{x}_k,\hat{f}_k,\boldsymbol{u}_k^c) = \hat{x}_k^T\Pi^T\mathcal{Q}\Pi\hat{x}_k;$$

where $\Pi$ and $\mathcal{Q}$ are defined after Eq. (14).

Now, by optimality, $V_N(\hat{x}_k,\hat{f}_k,\boldsymbol{u}_k^*) \leq V_N(\hat{x}_k,\hat{f}_k,\boldsymbol{u}_k)$ for any control sequence $\boldsymbol{u}_k$. Therefore:

$$V_N(\hat{x}_k,\hat{f}_k,\boldsymbol{u}_k^*) \leq V_N(\hat{x}_k,\hat{f}_k,\boldsymbol{u}_k^c) = \hat{x}_k^T\Pi^T\mathcal{Q}\Pi\hat{x}_k \leq c\|\hat{x}_k\|^2;$$

being $c$ the square of the maximum eigenvalue of $\Pi^T\mathcal{Q}\Pi$.

*Appendix B.2. Proof of inequality* (12)

At $t = t_k$, the optimal control sequence,

$$\mathbf{u}_k^* = [u_{k|k}^{*T},\ u_{k+1|k}^{*T},\ ...,\ u_{k+N-1|k}^{*T}]^T,$$

is obtained by solving (8).

This control sequence has the associated state-predictions $\mathbf{x}_k^* \triangleq [\hat{x}_{k|k}^{*\,T},\ \hat{x}_{k+1|k}^{*\,T},\ ...,\ \hat{x}_{k+N|k}^{*\,T}]^T$; which, by Eq. (5), satisfy:

$$\hat{x}^*_{k+j+1|k} = \Phi\hat{x}^*_{k+j|k} + \Gamma_1(u^*_{k+j|k}+\alpha\hat{f}_k); \quad \text{(B.3)}$$

being $\hat{x}^*_{k|k} \triangleq \hat{x}_k$ and $0 \leq j \leq N-1$.

For the next period, i.e. $t = t_{k+1}$, let us consider the following control sequence:

$$\mathbf{u}_{k+1}^c \triangleq [u_{k+1|k+1}^{c\,T},\ u_{k+2|k+1}^{c\,T},\ ...,\ u_{k+N|k+1}^{c\,T}]^T, = [u_{k+1|k}^{*T},\ ...,\ u_{k+N-1|k}^{*T},\ -(\alpha\hat{f}_{k+1}^T)]^T; \quad \text{(B.4)}$$

which, similarly, will have the associated state-predictions $\mathbf{x}_{k+1}^c \triangleq [\hat{x}_{k+1|k+1}^{c\,T},\ \hat{x}_{k+2|k+1}^{c\,T},\ ...,\ \hat{x}_{k+N+1|k+1}^{c\,T}]^T$; satisfying:

$$\hat{x}^c_{k+2+j|k+1} = \Phi\hat{x}^c_{k+1+j|k+1} + \Gamma_1(u^*_{k+j+1|k}+\alpha\hat{f}_{k+1}), \quad \text{for } 0 \leq j \leq N-2, \quad \text{(B.5a)}$$

$$\hat{x}^c_{k+N+1|k+1} = \hat{x}^c_{k+N|k+1}; \quad \text{(B.5b)}$$

with $\hat{x}^c_{k+1|k+1} \triangleq \hat{x}_{k+1}$.

Now, with $\mathbf{u}_k^*$ –and its associated predictions (B.3)– and with the next-period control sequence $\mathbf{u}_{k+1}^c$ –and its associated predictions (B.5)– let us show that:

$$V_N(\hat{x}_{k+1},\hat{f}_{k+1},\boldsymbol{u}_{k+1}^c) - V_N(\hat{x}_k,\hat{f}_k,\boldsymbol{u}_k^*) \leq - ||\hat{x}_k||_Q^2 + \Psi(||\tilde{y}_k||). \quad \text{(B.6)}$$

If (B.6) holds, then, by optimality, we have that $V_N(\hat{x}_{k+1},\hat{f}_{k+1},\mathbf{u}_{k+1}^*) \leq V_N(\hat{x}_{k+1},\hat{f}_{k+1},\boldsymbol{u}_{k+1}^c)$; being $\mathbf{u}_{k+1}^*$ the optimal control sequence that will be computed at the next period. This completes the proof.

In order to demonstrate (B.6), let us relate

$$V_N(\hat{x}_{k+1},\hat{f}_{k+1},\boldsymbol{u}_{k+1}^c) \triangleq \sum_{j=0}^{N-1}\left[||\hat{x}^c_{k+1+j|k+1}||_Q^2\right] + \sum_{j=0}^{N-1}\left[||u^c_{k+1+j|k+1}+\alpha\hat{f}_{k+1}||_R^2\right]+||\hat{x}^c_{k+N+1|k+1}||_P^2, \quad \text{(B.7)}$$

with

$$V_N(\hat{x}_k,\hat{f}_k,\mathbf{u}_k^*) \triangleq \sum_{j=0}^{N-1}\left[||\hat{x}^*_{k+j|k}||_Q^2\right] + \sum_{j=0}^{N-1}\left[||u^*_{k+j|k}+\alpha\hat{f}_k||_R^2\right]+||\hat{x}^*_{k+N|k}||_P^2, \quad \text{(B.8)}$$

To this end, it may be noted that Eqs. (B.3) and (B.5) can be related if one considers the observer equation (4), and that the control action introduced to the system is $u_k = u^*_{k|k}$ –i.e. Eq. (7). This permits to prove that:

$$\hat{x}^c_{k+1+j|k+1} = \hat{x}^*_{k+1+j|k} + \Psi_j\tilde{y}_k; \quad 0 \leq j \leq N-1, \quad \text{(B.9a)}$$

$$\hat{x}^c_{k+N+1|k+1} = \Phi\hat{x}^*_{k+N|k} + \Phi\Psi_{N-1}\tilde{y}_k \quad \text{(B.9b)}$$

being $\Psi_j \triangleq \Phi^jL_x + \sum_{i=0}^{j-1}\Phi^i\Gamma_2L_f$ and $\tilde{y}_k = y(t_k) - C\hat{x}_k$.

By substituting (B.4) and (B.9) into (B.7), it results:

$$V_N(\hat{x}_{k+1}, \hat{f}_{k+1}, \boldsymbol{u}^c_{k+1}) = \sum_{j=0}^{N-1} \left[||\hat{x}^*_{k+1+j|k} + \Psi_j \tilde{y}_k||^2_Q\right] + \sum_{j=0}^{N-2} \left[||u^*_{k+1+j|k} + \alpha \hat{f}_{k+1}||^2_R\right] + ||\Phi \hat{x}^*_{k+N|k} + \Phi\Psi_{N-1}\tilde{y}_k||^2_P. \tag{B.10}$$

Due to the triangular inequality, there exist class $\mathcal{K}_\infty$-functions, $\alpha_j(||\tilde{y}_k||)$, $\Upsilon_j(||\tilde{y}_k||)$ and $\gamma(||\tilde{y}_k||)$; such that:

$$\begin{aligned} &||\hat{x}^*_{k+1+j|k} + \Psi_j \tilde{y}_k||^2_Q \leq ||\hat{x}^*_{k+1+j|k}||^2_Q + \alpha_j(||\tilde{y}_k||), \\ &||u^*_{k+1+j|k} + \alpha \hat{f}_{k+1}||^2_R \leq ||u^*_{k+1+j|k} + \alpha \hat{f}_k||^2_R + \Upsilon_j(||\tilde{y}_k||), \\ &||\Phi \hat{x}^*_{k+N|k} + \Psi_{N-1}\tilde{y}_k||^2_P \leq ||\Phi \hat{x}^*_{k+N|k}||^2_P + \gamma(||\tilde{y}_k||); \end{aligned} \tag{B.11}$$

where $||u^*_{k+1+j|k} + \alpha \hat{f}_{k+1}||^2_R = ||(u^*_{k+1+j|k} + \alpha \hat{f}_k) + \alpha L_f \tilde{y}_k||^2_R$ has been employed in the second one.

By (B.8), (B.10), and (B.11), it holds that:

$$\begin{aligned} V_N(\hat{x}_{k+1}, \hat{f}_{k+1}, \boldsymbol{u}^c_{k+1}) - V_N(\hat{x}_k, \hat{f}_k, \boldsymbol{u}^*_k) \leq &-||\hat{x}_k||^2_Q \\ &- ||u^*_{k|k} + \alpha \hat{f}_k||^2_R + ||\Phi \hat{x}^*_{k+N|k}||^2_P - ||\hat{x}^*_{N+k|k}||^2_P \\ &+ ||\hat{x}^*_{N+k|k}||^2_Q + \Psi(||\tilde{y}_k||); \end{aligned}$$

where

$$\Psi(||\tilde{y}_k||) \triangleq \sum_{j=0}^{N-1} \left[\alpha_j(||\tilde{y}_k||)\right] + \sum_{j=0}^{N-2} \left[\Upsilon_j(||\tilde{y}_k||)\right] + \gamma(||\tilde{y}_k||).$$

Finally, as $R \geq 0$ and the terminal-cost weighting matrix $P$ has been restricted to be the solution to the Ricatti equation $\Phi^T P \Phi - P + Q = 0$; we have that $||u^*_{k|k} + \alpha \hat{f}_k||^2_R \geq 0$ and that $||\Phi \hat{x}^*_{k+N|k}||^2_P - ||\hat{x}^*_{k+N|k}||^2_P + ||\hat{x}^*_{N+k|k}||^2_Q = 0$. This proves (B.6).